Spontaneous Emergence of Large Scale Cell Cycle Synchronization in Amoeba Colonies

Igor Segota, Laurent Boulet & Carl Franck

Laboratory of Atomic and Solid State Physics, Cornell University, Ithaca, NY 14853, USA

Unicellular eukaryotic amoebae *Dictyostelium discoideum* are generally believed to grow in their vegetative state as single independent cells until starvation, when their social aspect emerges and they differentiate to form a multicellular slime mold. While major efforts continue to be aimed at their starvation-induced social aspect, our understanding of population dynamics and cell cycle in the vegetative growth phase has remained incomplete. Here we show that cell populations grown on a substrate spontaneously synchronize their cell cycles within several hours. These collective population-wide cell cycle oscillations span millimeter length scales and can be completely suppressed by washing away putative cell-secreted signals, implying signaling by means of a diffusible growth factor or as we argue as more likely, a mitogen. These observations give strong evidence for collective proliferation behavior in the vegetative state. This replaces the general view of these eukaryotes as independently growing cells in their vegetative phase and demonstrates a simple example of multicellular eukaryotic life.

Key words: cell cycle, cell growth, Dictyostelium discoideum, collective behavior

Submitted to PNAS, 6/3/13

Introduction

Collective oscillations of entire populations characterize many biological processes such as synchronized flashing of fireflies [1], glycolytic oscillations in yeast [2], cell aggregation in amoebae [3], circadian rhythms in cyanobacteria [4], [5], somite segmentation in zebrafish embryos [6], nuclear division in multinuclear HeLa cells [7] and synchronized cleavage divisions in *Xenopus* frog embryos [8]. These cooperative interactions can provide a fitness advantage, e.g. in cases when the environment is depleted of nutrients [3] or to assist in mate finding [1]. Recently, there has been a substantial progress in synthetic biology with the goal of engineering oscillatory genetic networks [9] and coupling them by quorum sensing [10]. In this work, however, the focus is on naturally emergent collective behavior in a model unicellular eukaryote, *Dictyostelium discoideum*. In nature, *D. discoideum* lives in the soil and feeds on bacteria in what is generally viewed as a solitary vegetative growth state [11]. When starved of nutrients they transition to a

collective state by chemotactically grouping into multicellular aggregates of 10^5 cells, eventually differentiating into stalk and spore cells, forming a lifeboat for their genomes. However, unlike in yeast *S. cerevisiae* [12] or *Xenopus* [13], very little is known about *D. discoideum* cell cycle in vegetative phase, mainly due to the lack of markers distinguishing different cell cycle phases: the first live-cell S-phase marker has only recently been introduced in *D. discoideum* [14].

Results

We studied *D. discoideum* population dynamics on glass substrates. A typical example of the dynamics of the average cell surface density in the exponential part of the vegetative phase was obtained by automated counting (Fig. 1a). Potentially interesting features are any deviations from pure exponential growth that do not result from uncertainty in counting. Here, the initial cell count is 40 ± 2 cells, spread out uniformly over a 4 mm^2 viewing area. During 26 hours, the cells did not move significantly (200 µm) compared our 2.3 mm × 1.8 mm recording area, resulting in patchy growth (Fig. 1b) further investigated in [15].

First, we show that the deviations from exponential growth (Fig. 1a) indeed represent signatures of collective cell divisions, by measuring the time dynamics of cell size distribution (Fig. 1c). This approach was used recently to quantify induced cell synchronization [16]. The time dynamics of cell size distributions (Fig. 1c) shows a clear periodic pattern, demonstrating partial synchrony in cell growth. To ensure that this is not a lineage effect (i.e. a low number subpopulation), we show the entire viewing area binned into 27 µm wide squares, with each bin color-coded by the local cell size and averaged over 1-2 cells (Fig. 1d). This demonstrates that synchronization in cell growth is not localized to a particular patch, thereby excluding any possibility of a lineage effect alone causing the large-scale oscillations. The cell-to-cell variation in doubling times is 7.3 ± 0.8 hours (Fig. S2) which is reflected in a strong lineage effect in a monoclonal population (see SI).

Next, we ensured that this periodic growth correlates with cell divisions. We manually annotated all cell division events, omitting initial events corresponding to declustering of cell clusters and cytokinesis of multinuclear cells present in suspension cultures [17], only counting single cell splitting into two, preceded by rounding up at the onset of cytokinesis. These manual annotations agree within < 1% to automated counts: for the data presented in Fig. 1, we counted 343 cell division events compared to 344 particles detected by automated counting (excluding initial declustering events). The cell division dynamics shows clear pulses (Fig. 1e) correlated with cell growth pattern. Furthermore, each collective cell division pulse (colored dots, Fig. 1e) is not localized to a particular patch (Fig. 1f). However, this still does not exclude the possibility of spontaneous synchronization in suspension cultures which was used to grow cells before plating.

The cells grown in suspensions have a broader size distribution (Fig. 2a) than those on substrates, consistent with previous observations of cell clusters [18] and multinuclear cells [17], since the lack of solid substrate probably impedes cytokinesis. These are all counted as a single particle by automated counting (Fig. 1a), however they are easily discriminated by cell size (particles between 150 and 300 μm^2 in Fig. 1c). Measurements of the cell size distribution dynamics in suspension cultures show no periodic growth (Fig. 2b), consistent with previous observations in development of *D. discoideum* synchronization protocols [19] [20] showing no evidence for suspension cell synchronization. In addition, our other experiments more clearly demonstrate the onset of synchronization on substrates (Fig. S1).

Nevertheless, one might wonder whether this synchronization is an artifact of simultaneous cytokinesis of multinuclear cells and cell cluster disintegration, resulting in a sudden large increase in the number of single cells. We observed that multinuclear cells undergo cytokinesis and clusters disintegrate uniformly in time throughout the first 6 hours after plating. This is also reflected in the fact that do not observe a sudden large increase in the single cell number after initial incoherent period (Figs. 1 and S1), demonstrating that cell synchronization is not induced by plating.

Next, we investigate the possibility that cells secrete a growth factor or a mitogen that serves as a synchronization signal. We analyzed the microfluidic experiments we performed previously [18] with cells grown on a substrate in a PDMS microfluidic device (Fig. 2c). In these experiments the cells naturally adhered to the glass while fresh growth medium flowed above them with 0.6, 1.7 and 17 μm/s flow speeds. If the synchronization signal is a small signaling molecule with diffusion coefficient about 300 $\mu m^2/s$, then these flow speeds correspond to Peclet numbers (see SI), quantifying the ratio of advective to diffusive transport, on the order of 0.4 (diffusion dominated), 1 and 10 (advection dominated), respectively [18]. Again, we measured both the cell density dynamics (Fig. 2d) and the cell size distribution dynamics (Fig. 2e). This qualitatively demonstrates the loss of coherence with increasing flow speed. However, it does not quantify the degree of collective coherence or measure the population fraction locked into this collective rhythm.

In order to quantify the collective synchronization of N cells, we represented the cell cycle position of cell j as a unit vector in complex plane at angle θ_j (Fig. 3a). The collective cell cycle oscillations are then represented as N points running around a unit circle. The "order parameter" $z = re^{i\psi} = \frac{1}{N}\sum_{j=1}^{N} e^{i\theta_j}$ is a vector of the centroid of these N points whose radius r represents the degree of collective phase coherence and measures the oscillation magnitude of the entire population. If all the cells oscillate in unison, then the points are clustered together resulting in r = 1. For random phased cell oscillations, r is smaller but unlikely to approach zero unless N is very large. To address this, we calculated the average and the standard deviation of r for N randomly phased oscillators (SI).

Since cell growth and division are correlated in *D. discoideum* (comparing Figs. 1d and 1e), we defined the cell cycle phase θ_j to be proportional to the cell size a_j, i.e. $\theta_j = \frac{2\pi}{a_{max}-a_{min}}\left(a_j - a_{min}\right)$, with the minimum and maximum cell size approximated from the cell size distributions to be given by a_{min} = 80 μm^2 and a_{max} = 150 μm^2 (the results are robust with respect to changing limits a_{min} and a_{max}). The phase coherence r for the experiment analyzed in Fig. 1 shows periodic oscillations (Fig. 3b) which reflects the fact that the cell size distribution broadens between each collective cell division pulse. The peak to peak variation in r is about 0.15, with the observed maxima well above the expected value for an incoherent system of the same number of cells and minimum values corresponding to complete incoherency. However, in other experiments there remained some residual level of coherence at the minima (Figs. S1b and S1d). The amplitude of r variation is considerably greater in monoclonal experiments, which is about 0.6 (Fig. S3b). The oscillations in r are possibly a consequence of the fact that while cell growth and division are coordinated, they are still separate processes and the synchronization signal might be a mitogen pulse that initiates cell division but does not persist throughout the majority of the cell cycle. We also calculated the phase coherence for the microfluidic flow experiments and again confirm the loss of coherence with increasing flow speed – the phase coherence approaches the values expected for randomly phased oscillators (Fig. 3c). While the true cell cycle phase is more precisely defined through the appearance of particular sets of cyclin proteins [21], no corresponding live-cell markers are available in *D. discoideum*. However, it is still very unlikely that using the "true" relation for $\theta_j(a_j)$ would erase all trace of the coherence observed here (Figs. 3b, 3c and S1).

Discussion

Collective synchronization has been theoretically studied in various versions of the simple Kuramoto model [22], [23], [24]. The solution for the Kuramoto model for finite oscillator number predicts sustained coherence with increasing cell number, consistent with our shorter 25-hour data (Fig. 3b), but inconsistent with our longer 40-hour experiments (Fig. S1). In addition, the observed feature of oscillating phase coherence (even if only in cell size) is not predicted by any of the Kuramoto models. These models assume that the coupling strength scales inversely with the number of oscillators, an assumption which needs to be changed in order to make realistic predictions for this system. Here, at least for short times, we expect that the coupling strength is diffusion limited and independent of cell number. A more appropriate description of the synchronized dynamics presented here would also predict a spatial dependence of phase coherence. The onset of synchronization observed here (Figs. 1c, 3b and S1) occurs within few hours which is consistent with the approximately 4 hour time needed for a small molecule with a diffusion coefficient of 300 μm^2/s to diffuse a distance of 2 mm and thereby cover the entire viewing field.

There is evidence for quorum sensing factors [18], [25], growth factors and factors repressing cell proliferation in *D. discoideum* [26], [27], [28] and their potential role in synchronization remains to be

determined. But, in fact, in our monoclonal experiments (Fig. S2a and S2b) we see no sign of a reduced cell proliferation rate even at the lowest possible cell densities. This is in stark contrast to bulk suspension systems where it has been argued that a slow-to-fast proliferation transition might be due to a diffusible growth factor [18]. However, unlike in bulk suspensions [18], here we see no evidence of a density dependent proliferation rate transition on surfaces (Fig. S2a and S2b) and this represents a new result. Therefore, a mitogen-type checkpoint is a much more likely explanation for the collective synchronization and seems unrelated to a density dependent proliferation transition in the bulk.

Furthermore, we speculate as to the possible purpose of these oscillations. It is known that during starvation, *D. discoideum* cells differentiate into prestalk and prespore cells, a process which correlates with cell cycle positions [29], [30]. Since only spore cells potentially survive, there is a competition to form spores. If the cell fate is determined by its cell cycle position, the synchronized fraction could be collectively turned into either prestalk or prespore cells and possibly more effectively competes for becoming a spore.

In summary, it is remarkable that a large scale collective aspect of life was hidden within this seemingly non-interacting system of unicellular microbes (Fig. 1a). The absence of synchronized growth in suspensions might be caused by the fact that the lack of substrate introduces a stochastic delay of cytokinesis by a time that is difficult to estimate. As we indicated, these observations are ripe for quantitative modeling and present elegant challenges: macro-scale synchronization of proliferating oscillators where the micro-scale oscillator is the proliferation process itself. Future experimental work will reveal how universal this phenomenon is. From a practical standpoint, it presents insight into the problem of cell culturing for stem cell development and large scale parallel bioassays where the difficulty of very dilute cell culture arises, as discussed in [18]. It also demands better appreciation of the importance of the nonliving culture environment: flowing suspension vs. hydrophilic substrates with or without fluid flow. Equally interesting are the biochemical circuits in play, e.g. the timing pattern of the chemical signals that cells are apparently exchanging. Returning to the theoretical challenges, while we have argued that our observations reveal a collective proliferation waves that already encompassed the entire field of view (Fig. 1b and 1d), our understanding of the spatial dynamics of these waves remains an open question.

Materials and Methods

Dictyostelium discoideum wild-type AX3 and AX4 axenic strains were grown in HL5 with glucose suspension culture (ForMedium, UK) with 250 µl PenStrep (Invitrogen) per 25 ml flask. No variation in results was noticed with cell culturing for up to one year. Cells were grown in exponential phase on an orbital shaker (150 rpm) in standard 25 ml Erlenmeyer flasks to 10^5 or 10^6 cells/ml (21ºC). For substrate growth, these cultures were transferred to fresh HL5, diluted to 10^3-10^5 cells/ml and 300 µl samples were plated on hydrophilic MatTek (P50G-1.5-14-F) glass bottom dishes. Recording was performed in bright

field with an inverted Olympus IX71 or an upright Nikon Optiphot (4X objective both) within 15 minutes of plating. Images were taken every 5 minutes using a Home Science Tools camera MI-DC5000 or a Logitech QuickCam Pro 4000. The Olympus/Home Science combination provided better resolution (Figs. 1 and S1) than the Optiphot/Logitech system (Fig. S1c). For suspension growth, flasks ware sampled hourly for 11-12 hours, by injecting a 20 µl sample into a hemocytometer and ~20 image sets were taken within 3 minutes.

Background was removed using ImageJ (NIH) by subtracting the average of all images from each frame (for each experiment). Particles were detected and counted using ImageJ by thresholding. Cell sizes were measured using the "Analyze particles" tool. Centroids of particles were used as cell coordinates (Figs. 1c, 1d and 1f). Microfluidic experiments including imaging systems used were described previously [18]. Briefly, polydimethylsiloxane (PDMS) microfluidic device was employed with continuous flow of fresh HL5 growth medium over 2 mm × 2 mm × 200 µm chamber, containing exponential growth phase AX3 cells. Frames were recorded every 15 minutes for 16-40 hours. Images were analyzed as described previously. The doubling times were 8-11 hours, consistent with the usual suspension culturing.

Acknowledgments

We thank Dicty Stock Center; Northwestern University for AX3 and AX4 cell lines and Cornell Center for Materials Research for use of the facilities funded by the National Science Foundation under grant DMR-1120296.

Author Contributions

I.S. designed the study. I.S., L.B., and C.F. performed the experiments. I.S. and C.F. analyzed the data and wrote the manuscript.

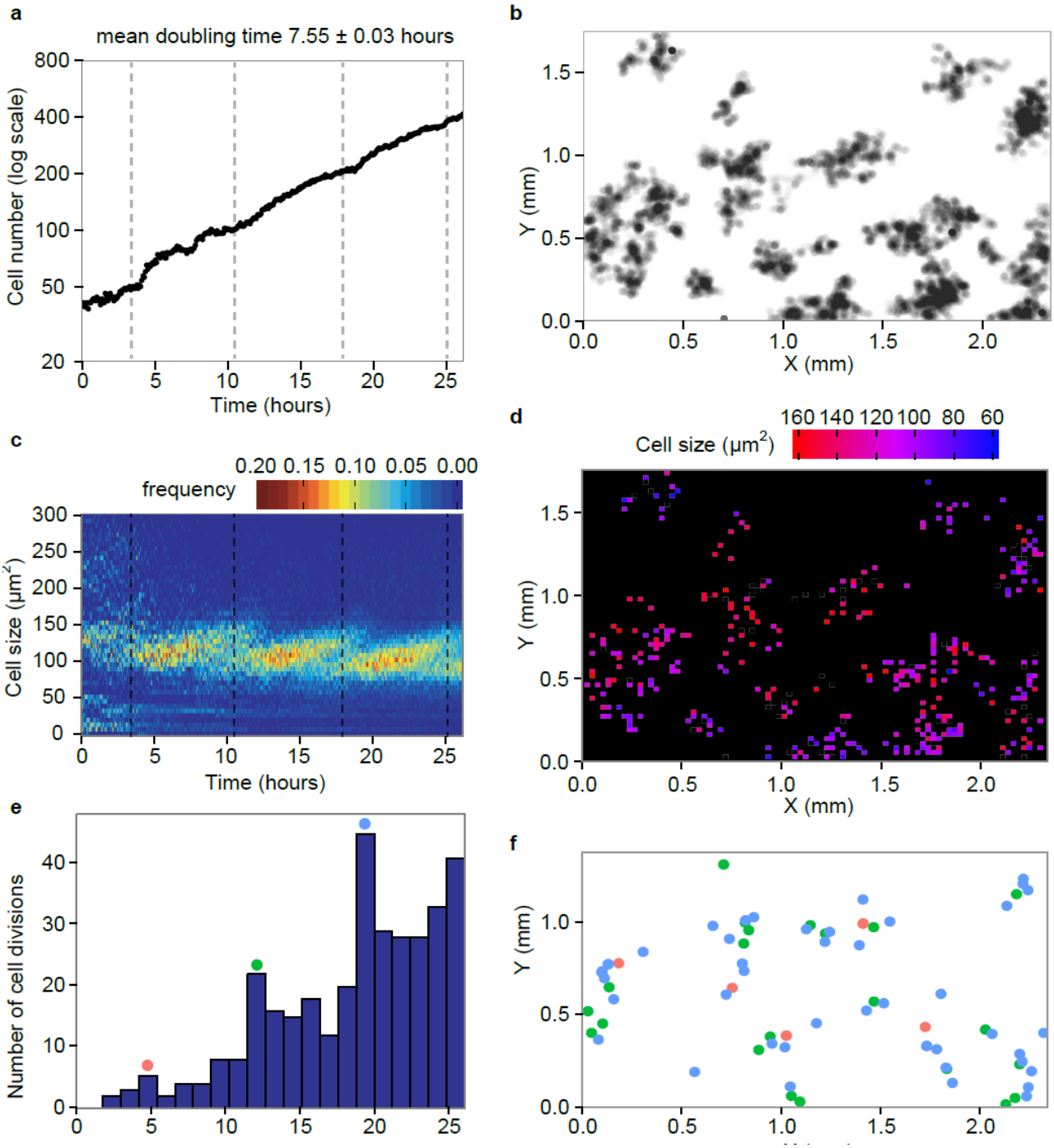

Figure 1. **Synchronization of cell growth on a substrate. a**, Growth dynamics of proliferating cells. **b**, Strobe (at 5 minute intervals over 26 hours) image of cell positions; darker areas correspond to more visited locations. **c**, Dynamics of cell size distribution. The sudden jumps are marked by dashed lines and extrapolated to a. **d**, Spatial distribution of cells at 25 hours with color representing cell size. **e**, Number of cell divisions in 1.2-hour intervals. Peaks in cell divisions correlate with sudden jumps in the cell size distribution shown in part b. **f**, Spatial distribution of the three cell division peaks from e.

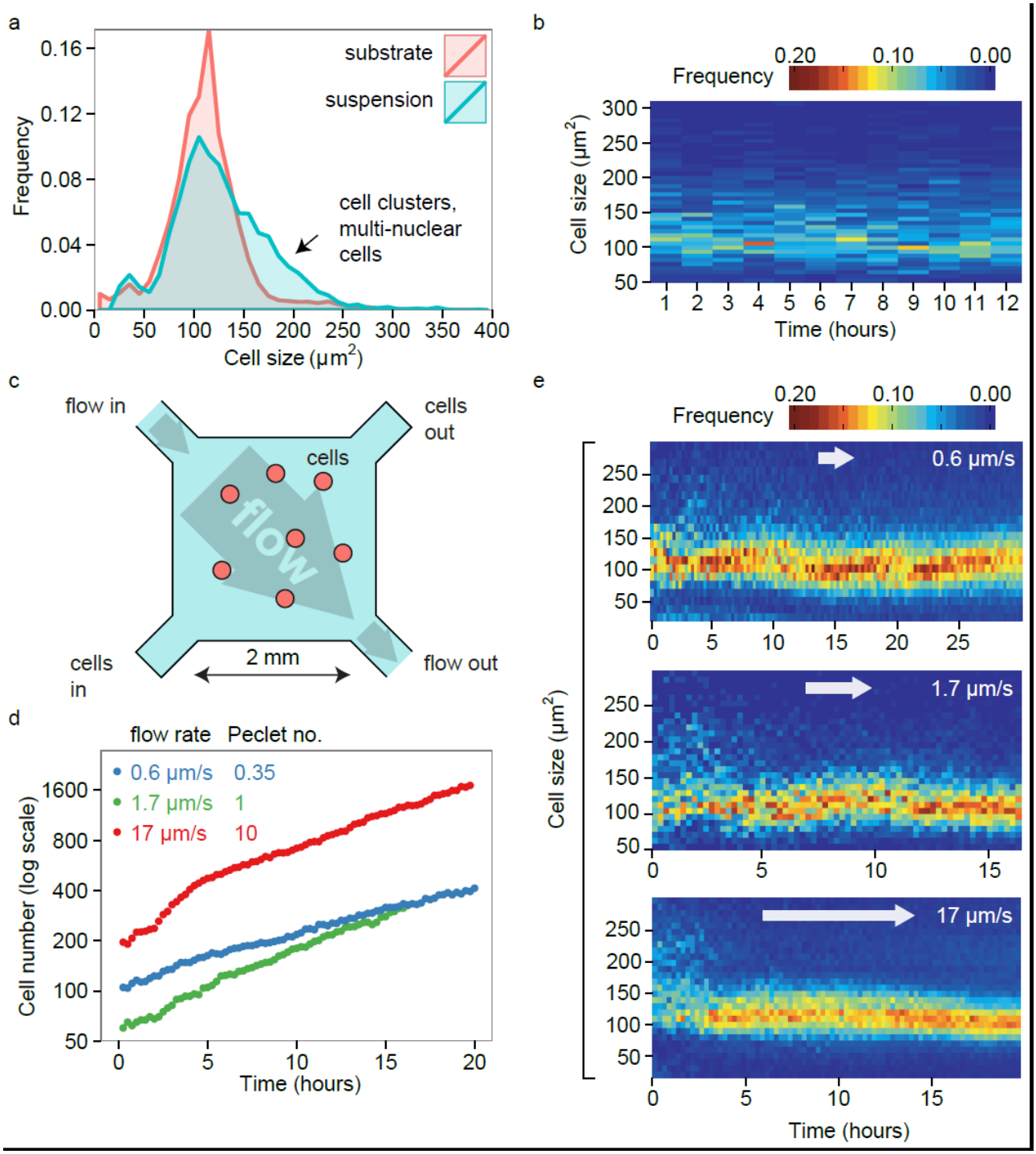

Figure 2. **Suspension culture growth and microfluidic flow experiments. a,** Time averaged cell size distributions for substrate and suspension growth. **b,** Time course of cell size distribution in suspension. **c,** Schematic of the microfluidic devices employed for flow experiments. **d,** Growth dynamics in flow experiments. **e,** Time course of cell size distributions for substrate flow experiments.

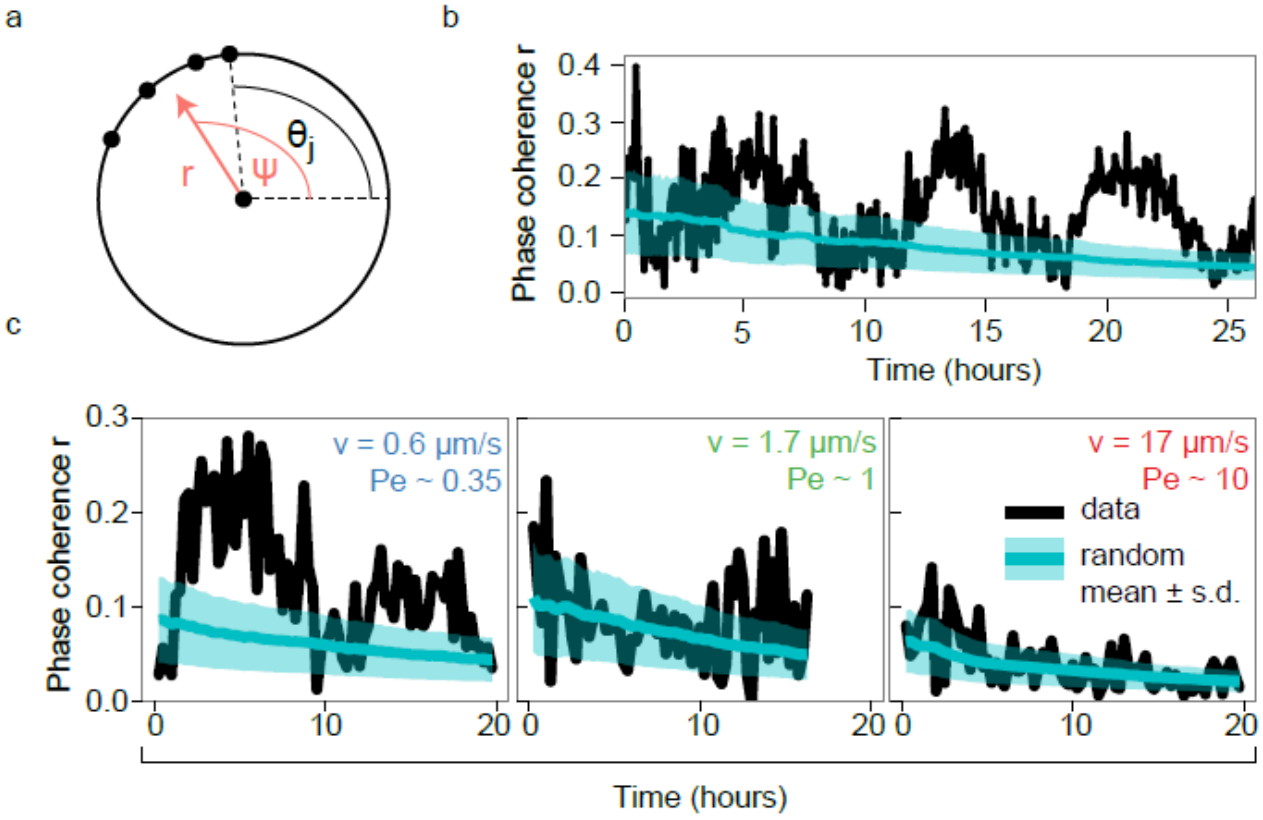

Figure 3. **Quantitative analysis of oscillations**. **a,** Phase coherence r, a number between 0 and 1, is defined as a magnitude of the vector sum of N unit vectors each having an angle θ_j, divided by N (shown in red). The angle ψ describes the phase of the collective oscillation. **b,** Phase coherence for the experiment in Fig. 1. The cells periodically go in and out of coherence. **c,** Phase coherence for microfluidic flow experiments, demonstrating the loss of coherence at higher flow speeds. The cyan line and its spread denote the average and standard deviation for random-phase systems (see SI).

Supporting Information (4 files)

Supporting Information text

Supporting Information Text is submitted in MS Word format with this manuscript submission.

Supporting Figure Legends

References

1. Buck J & Buck E (1968), Mechanism of Rhythmic Synchronous Flashing of Fireflies. Science 159:1319-1327.

2. De Monte S, d'Ovidio F & Sorensen PG (2007), Dynamical quorum sensing: Population density encoded in cellular dynamics. PNAS 104:18377–18381.

3. Sawai S, Thomason PA & Cox EC (2005), An autoregulatory circuit for long-range self-organization in Dictyostelium cell populations. Nature 433:323-326.

4. Mihalcescu I, Hsing W & Leibler S (2004), Resilient circadian oscillator revealed in individual cyanobacteria. Nature 430:81-85.

5. Yang Q, Pando BF, Dong G, Golden SS & van Oudenaarden A (2010), Circadian Gating of the Cell Cycle Revealed in Single Cyanobacterial Cells. Science 327:1522-1526.

6. Horikawa K, Ishimatsu K, Yoshimoto E, Kondo S & Takeda H (2006), Noise-resistant and synchronized oscillation of the segmentation clock. Nature 441:719-723.

7. Rao PN & Johnson RT (1970), Mammalian Cell Fusion: Studies on the Regulation of DNA Synthesis and Mitosis. Nature 225:159-164.

8. Kirschner M, Newport J & Gerhart J (1985), The timing of early developmental events in Xenopus. Trends Genet. 1:41-47.

9. Elowitz MB & Leibler S (2000), A synthetic oscillatory network of transcriptional regulators. Nature 403:335-338.

10. Danino T, Mondragon-Palomino O, Tsimring L & Hasty J (2010), A synchronized quorum of genetic clocks. Nature 463:326-330.

11. Kessin RH (2001) Dictyostelium: Evolution, Cell Biology and the Development of Multicellularity Cambridge, UK:Cambridge University Press.

12. Cai L & Tu BP (2012), Driving the Cell Cycle Through Metabolism. Annu. Rev. Cell Dev. Biol. 28:59-87.

13. Philpott A & Yew RP (2008), The Xenopus Cell Cycle: An Overview. Mol. Biotechnol. 39:9-19.

14. Muramoto T & Chubb JR (2008), Live imaging of the Dictyostelium cell cycle reveals widespread S phase during development, a G2 bias in spore differentiation and a premitotic checkpoint. Development 135:1647-1657.

15. Houchmandzadeh B (2008), Neutral Clustering in a Simple Experimental Ecological Community. Phys. Rev. Lett. 101:078103.

16. Tzur A, Kafri R, LeBleu VS, Lahav G & Kirschner MW (2009), Cell Growth and Size Homeostasis in Proliferating Animal Cells. Science 325:167-171.

17. Waddell DR, Duffy K & Vogel G (1987), Cytokinesis Is Defective in Dictyostelium Mutants with Altered Phagocytic Recognition, Adhesion, and Vegetative Cell Cohesion Properties. J. Cell Biol. 105:2293-2300.

18. Franck C, Ip W, Bae A, Franck N, Bogart E et al. (2008), Contact-mediated cell-assisted cell proliferation in a model eukaryotic single-cell organism: an explanation for the lag phase in shaken cell culture. Phys Rev E 77:041905.

19. Maeda Y (1986), A New Method for Inducing Synchronous Growth of Dictyostelium discoideum Cells Using Temperature Shifts. Microbiology 132:1189-1196.

20. Weijer CJ, Duschl G & David CN (1984), A revision of the Dictyostelium discoideum cell cycle. J. Cell Sci. 70:111-131.

21. Murray AW (2004), Recycling the Cell Cycle: Cyclins Revisited. Cell 116:221-234.

22. Kuramoto Y & Nishikawa I (1987), Statistical Macrodynamics of Large Dynamical Systems. Case of a Phase Transition in Oscillator Communities. J. Stat. Phys. 49:569-605.

23. Acebron JA, Bonilla LL, Perez Vicente CJ, Ritort F & Spigler R (2005), The Kuramoto model: A simple paradigm for synchronization phenomena. Rev. Mod. Phys. 77:137-185.

24. Strogatz SH (2000), From Kuramoto to Crawford: exploring the onset of synchronization in populations of coupled oscillators. Physica D 143:1-20.

25. Gole L, Riviere C, Hayakawa Y & Rieu J-P (2011), A Quorum-Sensing Factor in Vegetative Dictyostelium Discoideum Cells Revealed by Quantitative Migration Analysis. PLoS ONE 6.

26. Gomer RH, Jang W & Brazill D (2011), Cell density sensing and size determination. Develop. Growth

Differ. 53:482-494.

27. Brock DA & Gomer RH (2005), A secreted factor represses cell proliferation in Dictyostelium. Development 132:4553-4562.

28. Whitbread JA, Sims M & Katz ER (1991), Evidence for the presence of a growth factor in Dictyostelium discoideum. Dev. Genet. 12:78-81.

29. Araki T, Nakao H, Takeuchi I & Maeda Y (1994), Cell-cycle-dependent sorting in the development of Dictyostelium cells. Dev. Biol. 162:221-228.

30. Wood SA, Ammann RR, Brock DA, Spann T & Gomer RH (1996), RtoA links initial cell type choice to the cell cycle in Dictyostelium. Development 122:3677-3685.

Spontaneous emergence of large scale cell cycle synchronization in amoeba colonies

SUPPLEMENTARY INFORMATION

Igor Segota, Laurent Boulet & Carl Franck

Laboratory of Atomic and Solid State Physics, Cornell University, Ithaca, NY 14853, USA

Probability distribution of phase coherence *r* for *N* random oscillators

We start by representing the size (area) of each cell by a unit vector with length $L = 1$ in complex plane $e^{i\theta_j}$ where j is the cell index. The probability distribution of each step is then:

$$p(\vec{r}_j) = p(r_j, \theta_j) = \frac{1}{2\pi L}\delta(r_j - L)$$

which is normalized:

$$\int_{\theta_j=0}^{2\pi}\int_{r_j=0}^{\infty} p(r_j, \theta_j) r_j dr_j d\theta_j = \int_{\theta_j=0}^{2\pi}\int_{r_j=0}^{\infty} \frac{1}{2\pi L}\delta(r_j - L) r_j dr_j d\theta_j = 1$$

where $\delta(r_j - L)$ is the Dirac delta function. The average and variance of a single step are:

$$\langle \vec{r}_j \rangle = \int \vec{r}_j p(\vec{r}_j) d\vec{r}_j = L \cdot 0 = 0$$

$$\sigma_{rj}^2 = \langle {r_j}^2 \rangle = \int {r_j}^2 \frac{1}{2\pi L}\delta(r_j - L) 2\pi r_j dr_j = L^2$$

Also note that:

$$\sigma_{xj}^2 = \frac{1}{2}\sigma_{rj}^2 = \frac{L^2}{2}, \quad \sigma_{rj}^2 = \sigma_{xj}^2 + \sigma_{yj}^2$$

Now for the average:

$$\vec{z} = \frac{1}{N}\sum_{j=1}^{N}\vec{r}_j, \;\; z_x = \frac{1}{N}\sum_{j=1}^{N} r_{xj}, \;\; z_y = \frac{1}{N}\sum_{j=1}^{N} r_{yj}$$

we can apply Central Limit Theorem for each x and y component individually (if N is large). Each Cartesian component x and y (of z) then has a Normal distribution with mean 0 and variance $\sigma_{xj}^2/N = L^2/(2N)$. The probability distribution of z is:

$$p(z_x, z_y) = Ae^{-\frac{z_x^2}{2\sigma_{xj}^2/N}} e^{-\frac{z_y^2}{2\sigma_{yj}^2/N}} = Ae^{-\frac{(z_x^2+z_y^2)}{2\sigma_{xj}^2}} = Ae^{-\frac{r^2}{L^2/N}}$$

where the normalization constant can be obtained by requiring that the integral of this probability is 1 and we evaluate the integral in polar coordinates r, ψ:

$$\int_{\psi=0}^{2\pi}\int_{r=0}^{\infty} Ae^{-\frac{r^2}{L^2/N}} r d\psi dr = 1 = 2\pi A\frac{L^2}{2N} = \frac{A\pi L^2}{N}, \quad A = \frac{N}{\pi L^2}$$

The average phase coherence for a random system can be directly calculated:

$$\langle r\rangle = \int_{\psi=0}^{2\pi}\int_{r=0}^{\infty} \frac{N}{\pi L^2} e^{-\frac{r^2}{L^2/N}} r^2 d\psi dr = \frac{\sqrt{\pi}}{2}\frac{L}{\sqrt{N}}$$

and the average of r^2 is:

$$\langle r^2\rangle = \int_{\psi=0}^{2\pi}\int_{r=0}^{\infty} \frac{N}{\pi L^2} e^{-\frac{r^2}{L^2/N}} r^3 d\psi dr = \frac{L^2}{N}$$

so the variance is $\sigma_r^2 = \langle r^2\rangle - \langle r\rangle^2 = \frac{L^2}{N} - \frac{\pi}{4}\frac{L^2}{N}$ and the standard deviation is:

$$\sigma_r = \frac{L}{\sqrt{N}}\sqrt{\frac{4-\pi}{4}}$$

which gives us the relative fluctuation:

$$\frac{\sigma_r}{\langle r\rangle} = \frac{\sqrt{\frac{4-\pi}{4}}}{\frac{\sqrt{\pi}}{2}} = \sqrt{\frac{4}{\pi} - 1} \approx 0.52$$

In Fig.3 in the main text we make use of $\langle r\rangle$ and σ_r to show the average and the standard deviation for the phase coherence for finite populations.

Additional examples of cell synchronization

Here we show two more examples indicating an onset of synchronized growth (Fig.S1). The cell synchronization occurs very quickly, within the first several hours. The runs also reveal longer time behavior than in Fig. 3, indicating decay of coherence at long times (see discussion in the main text).

Estimate of the Variation of the Degree of Coherence with Increasing Number of Cells

We can estimate of the effect of cell proliferation on the degree of cell cycle synchronization according to the Kuramoto model. Recent efforts to explore the phenomenon of synchronization of many oscillators have focused of extensions of the Kuramoto model to include explicit consideration of network topology, interaction strength and finite population. The problem at hand invites us to consider the last aspect: what are the dynamics of synchronization for a growing population? From the work of Hemmen and Wrenzinki, Ref. S1, we have the following equation for r, long time coherence of the system:

$$r = \sum_{\{\omega\}} p(\omega) \left[1 - \left(\frac{\Delta(\omega)}{K\, r}\right)^2\right]^{1/2} \quad \text{(SI-1)}$$

where the summation is over a collection of N oscillators whose unperturbed frequencies are given by the set $\{\omega\}$, the probability of each value of frequency is given by $p(\omega)$, K is the interoscillator coupling strength in the (infinitely-ranged) Kuramoto model (Eqn. 1 on p. 146 of Ref. S1) and $\Delta(\omega) \stackrel{\text{def}}{=} \omega - \langle\omega\rangle$ is the deviation of the frequency of a particular oscillator from the mean frequency of the entire set of oscillators, $\langle\omega\rangle$. We examine the dependence of r on N with a minimalist distribution: all the oscillators have either $\omega = \omega_0 + \delta$ or $\omega = \omega_0 - \delta$ with equal probability. Then we have the following equation for r:

$$r = \sum_{\{\omega\}} p(\omega) \left[1 - \left(\frac{\delta}{K\, r}\right)^2\right]^{1/2} = N \left(\frac{1}{N}\right) \left[1 - \left(\frac{\delta}{K\, r}\right)^2\right]^{1/2} = \left[1 - \left(\frac{\delta}{K\, r}\right)^2\right]^{1/2} \quad \text{(SI-2)}$$

We conclude that r is independent of N. We therefore do not expect the degree of coherence achieved at long times to vary as the cells proliferate.

Peclet numbers

Following the discussion in [S2] the Peclet number is the dimensionless number quantifying the ratio of advective and diffusive transport, defined as:

$$Pe = \frac{Lv}{D}$$

where L is a characteristic length, v is the advective flow speed and D is the diffusion coefficient of the particle being transported. In our analysis in the main text, we calculated the Peclet numbers for small molecules such as cAMP to help us get an idea what range of flow rates in microfluidic experiments are relevant to this study.

Synchronization in monoclonal populations and lineage effects

We investigated the degree of phase coherence in monoclonal populations, starting from a 1 cell per 4 mm^2 area, which is a minimal cell surface density achievable in our experimental setup. The mean and standard deviation of doubling times owing to cell-to-cell variation were 7.3 ± 0.8 hours. We determined this based on the experiment presented in Fig. 1 in the main text by manually tracking 55 cells (Fig. S2).

If the cell division is thought of as a random walk process with the mean $T_D = 7.3$ hours and standard deviation $\sigma = 0.8$ hours, we can estimate the number of generations needed for the complete loss of lineage effect. The number of generations n needed for the standard deviation $\sigma\sqrt{n}$ to become equal to the mean T_D is $n \approx 80$. This is due to the fact that the cell division clock is relatively precise with only about 10% error (Fig. S2b). The dynamics of cell size distribution and phase coherence for single-cell experiments are shown in Fig. S3 and, as expected, show very strong lineage effect.

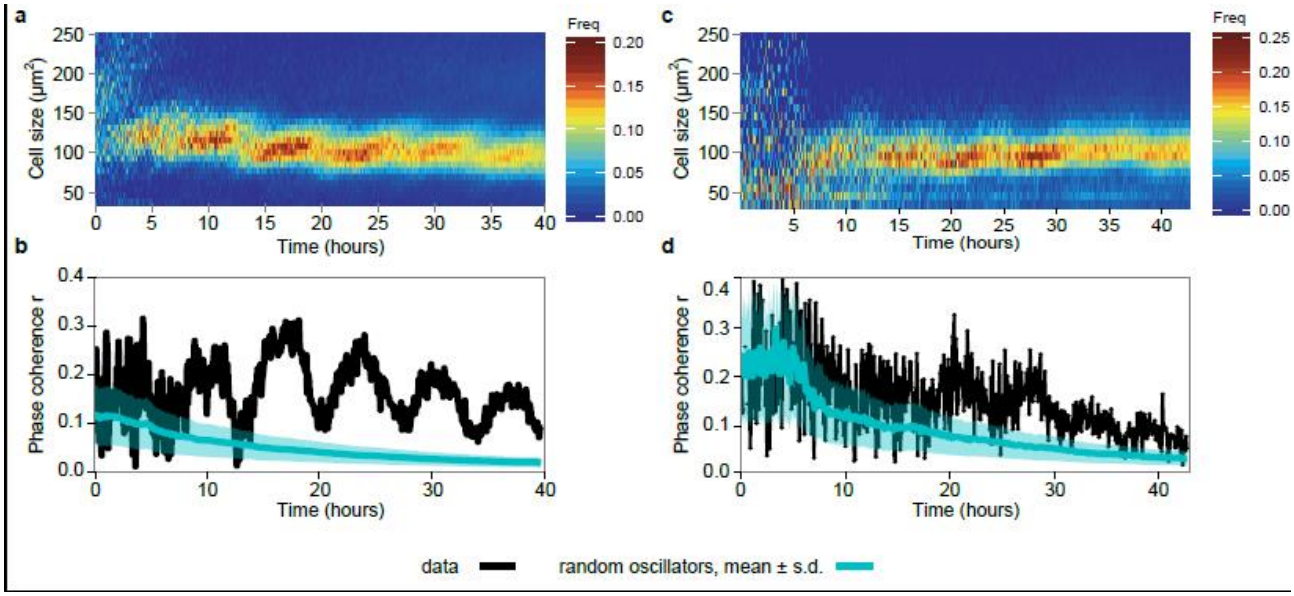

Figure S1. **Additional examples of synchronization in cell. a,b,** The dynamics of cell size distribution and phase coherence for the first experiment. **c,d**, The dynamics of cell size distribution and phase coherence for the second experiment. As in main text, black lines denote phase coherence in our data and cyan line and its spread shows the mean phase coherence and its spread for the corresponding number of randomly oscillating cells.

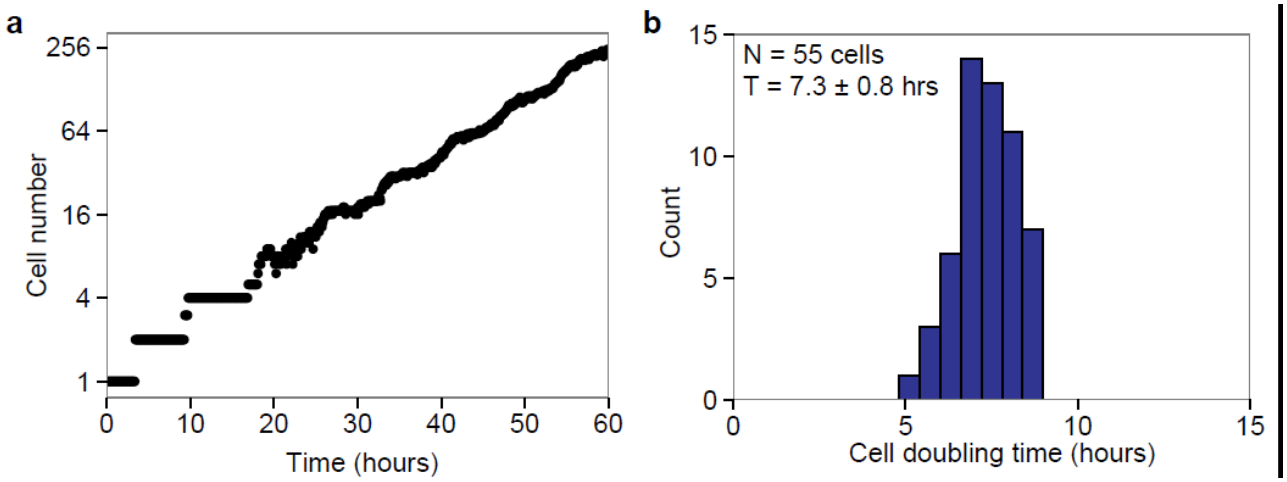

Figure S2. **Single cells growth. a,** Growth dynamics of single cell growth. **b,** Distribution of single cell doubling times showing cell-to-cell variability.

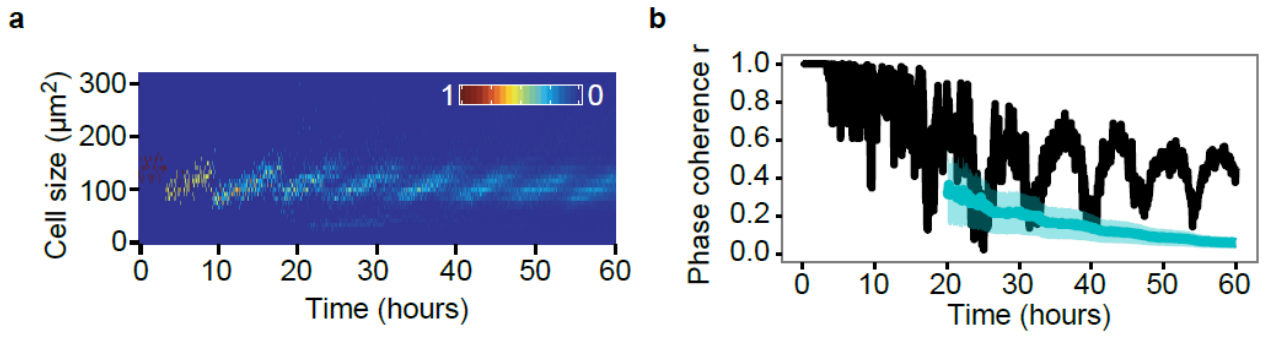

Figure S3. **Lineage effects in single cell growth. a,** Cell size distribution for a monoclonal population started from a single cell. **b,** Phase coherence for the same system showing the lineage effect. The cyan line and its spread denote the average and standard deviation for random-phase systems for large number of cells.

References:

S1) J.L. van Hemmen and W.F. Wreszinski, ``Lyapunov Function for the Kuramoto Model of Nonlinearly Coupled Oscillators," *J. Stat. Phys.*, vol. 72, pp. 145-166, 1993.

S2) C. Franck, W. Ip, A. Bae, N. Franck, E. Bogart and T. T. Le, "Contact-mediated cell-assisted cell proliferation in a model eukaryotic single-cell organism: an explanation for the lag phase in shaken cell culture.," *Phys Rev E,* vol. 77, p. 041905, 2008.